DOI: 10.1002/ejoc.200800228

Case Study on the Effects of Molecular Structure on the Mode of Polymorphic Transition Inducing Preferential Enrichment

Masahiro Horiguchi,[a] Shinsuke Yabunaka,[a] Sekai Iwama,[a] Eiji Shimano,[a] Zsolt Lepp,[a] Hiroki Takahashi,[a] Hirohito Tsue,[a] and Rui Tamura*[a]

Keywords: Chiral resolution / Polymorphism / Symmetry breaking / Chirality

A series of (±)-*N*-{2-[4-(2-hydroxy-3-ethoxypropoxy)phenylcarbamoyl]ethyl}-*N*-methylpyrrolidinium *p*-halobenzenesulfonates [(±)-**1a–c**] were found to cause an unusual symmetry-breaking enantiomeric resolution phenomenon called preferential enrichment, whereas the *N*-methylpiperidinium analogues (±)-*N*-{2-[4-(2-hydroxy-3-ethoxypropoxy)phenylcarbamoyl]ethyl}-*N*-methylpiperidinium *p*-halobenzenesulfonates [(±)-**2a–c**] failed to show this phenomenon. By X-ray crystallographic and ATR-FTIR spectroscopic studies, (±)-**1a–c** were found to undergo the desired solvent-assisted solid-to-solid polymorphic transition of the first-formed and metastable γ-form into the stable δ-form, which could induce preferential enrichment. In contrast, (±)-**2a–c** were subject to the undesired solvent-mediated polymorphic transition of the γ-form into the α_2-form, and similarly, (±)-**1d** and (±)-**2d** bearing a *p*-toluenesulfonate ion also showed the undesired solvent-mediated polymorphic transition of the γ-form into the β-form; in these cases, preferential enrichment was not observed. Accordingly, the structure of the cyclic ammonium group as well as the basicity of the *p*-substituted benzenesulfonate ion largely affected the mode of the polymorphic transition.

Introduction

Preferential enrichment is a symmetry-breaking dynamic enantiomeric resolution phenomenon that occurs during crystallization from the supersaturated solution of certain kinds of racemic mixed crystals (or solid solutions) composed of two enantiomers in the absence of any external chiral element.[1,2] We have been studying the relationship between the molecular structure and the occurrence of preferential enrichment. The molecular structure required for the occurrence of preferential enrichment is represented in Figure 1: (i) the amide, hydroxy, and terminal alkoxy groups in the long-chain cation are indispensable to form hydrogen bonds, (ii) the terminal alkoxy group is limited to a methoxy, ethoxy, or phenoxy group, and (iii) the onium sulfonate structure is advantageous for inducing polymorphism; the *p*-substituted benzenesulfonate ion with low basicity is appropriate for the occurrence of smooth polymorphic transition as shown below.[1–5]

The mechanism of preferential enrichment was found to include the following two key-processes during crystallization from the supersaturated solution: (i) A solvent-assisted solid-to-solid transformation of an initially formed metastable polymorphic form into a thermodynamically stable one. (ii) Concomitant partial crystal disintegration inside the transformed crystal lattice, which releases the excess enantiomer existing in the initial crystal into solution.[1–4,6,7] Thus far, three modes of solvent-assisted solid-to-solid polymorphic transition inducing preferential enrichment were found to occur, depending on the selection of the terminal R substituent in the long-chain cation and the *para* X substituent on the benzenesulfonate ion. For example, in the cases of R = Me and Et, the *transition a* (or *b*) from a γ-form to a δ-form (or an ε-form) occurs to induce preferential enrichment (Figure 2), whereas in the case of R = Pr, the polymorphic transition does not occur, because the steric hindrance fails to induce preferential enrichment.[3,8] Furthermore, in the cases of R = Ph and *p*-

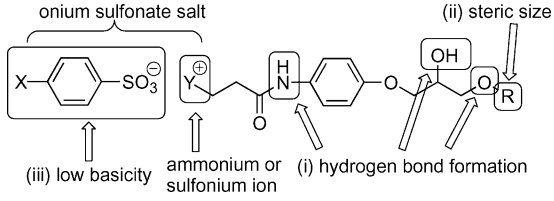

Figure 1. Structural requirements for showing preferential enrichment.

[a] Graduate School of Human and Environmental Studies, Kyoto University,
Kyoto 606-8501, Japan
Fax: +81-75-753-7915
E-mal: tamura-r@mbox.kudpc.kyoto-u.ac.jp

Supporting information for this article is available on the WWW under http://www.eurjoc.org/ or from the author.

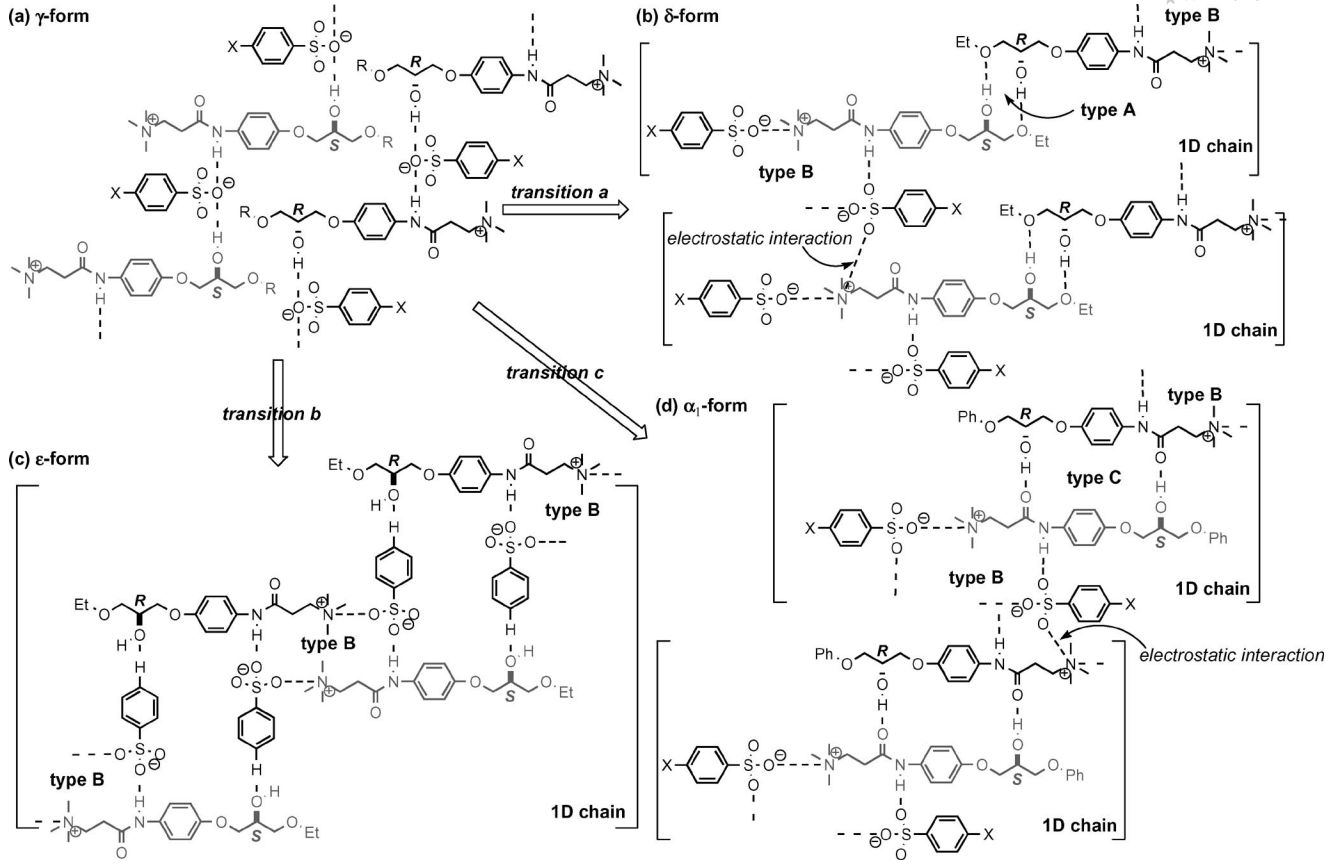

Figure 2. Supramolecular structures characteristic of (a) γ-form, (b) δ-form, (c) ε-form, and (d) α_1-form crystals.

FC_6H_4, the *transition c* from a γ-form to an α_1-form successfully occurs to induce preferential enrichment (Figure 2).[4,5]

To clarify the hitherto unknown relationship between the structure of the terminal ammonium group and the occurrence of preferential enrichment, we prepared a series of new compounds (±)-**1** and (±)-**2**, and their preferential enrichment experiments were performed (Figure 3 and Table 1). As a result, (±)-**1a**–**c** bearing an *N*-methylpyrrolidinium group and a *p*-halobenzenesulfonate ion showed preferential enrichment, whereas (±)-**2a**–**c** having an *N*-methylpiperidinium group and a *p*-halobenzenesulfonate ion failed to display the phenomenon. Neither (±)-**1d** nor (±)-**2d** with a more basic *p*-toluenesulfonate ion exhibited preferential enrichment. Here we report these experimental results and discuss each mode of polymorphic transition occurring during crystallization on the basis of X-ray crystal structures, powder X-ray diffraction patterns, and in situ ATR-FTIR spectra.

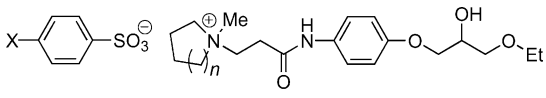

(±)-**1a**, X = Cl, *n* = 1 (±)-**2a**, X = Cl, *n* = 2
(±)-**1b**, X = Br, *n* = 1 (±)-**2b**, X = Br, *n* = 2
(±)-**1c**, X = I, *n* = 1 (±)-**2c**, X = I, *n* = 2
(±)-**1d**, X = Me, *n* = 1 (±)-**2d**, X = Me, *n* = 2

Figure 3. Compounds studied in this paper.

Table 1. Preferential enrichment and the mode of polymorphic transition for (±)-**1** and (±)-**2**.

Compound	Solubility in EtOH [mg mL^{-1}]	Preferentialen-richment	Mode of polymorphic transition
(±)-**1a**	207.5	yes[a]	γ to δ
(±)-**1b**	55.1	yes[a]	γ to δ
(±)-**1c**	45.0	yes[a]	γ to δ
(±)-**1d**	13.3	no[b]	γ to β
(±)-**2a**	141.0	no[b]	γ to α_2
(±)-**2b**	49.6	no[b]	γ to α_2
(±)-**2c**	44.4	no[b]	γ to α_2
(±)-**2d**	67.0	no[b]	γ to β

[a] Preferential enrichment occurred. [b] Preferential enrichment did not occur.

Results and Discussion

Preferential Enrichment of (±)-1 and (±)-2

The racemates of a series of cyclic *N*-methylammonium sulfonates [(±)-**1** and (±)-**2**] were prepared and recrystallized from EtOH under the standard experimental conditions for preferential enrichment. Consequently, (±)-**1a** and (±)-**1b** successfully exhibited preferential enrichment by crystallization from their three- and sevenfold supersaturated solutions, respectively (Figures 4 and 5). Although (±)-**1c** also exhibited preferential enrichment, 15-fold supersaturation and three or four weeks were required and the reached *ee* value was at most 65% (Figure 6). In contrast, the *N*-methylpiperidinium analogues (±)-**2a**–(±)-**2c** and the *p*-toluenesulfonate analogues (±)-**1d** and (±)-**2d** failed to show preferential enrichment.

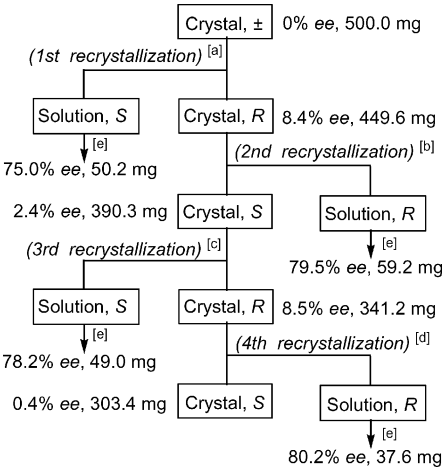

Figure 4. Preferential enrichment of (±)-**1a**. Conditions: [a] EtOH (0.8 mL), –20 °C, 7 d; [b] EtOH (0.7 mL), –20 °C, 7 d; [c] EtOH (0.6 mL), –20 °C, 7 d; [d] EtOH (0.5 mL), –20 °C, 7 d; [e] removal of the solvent by evaporation.

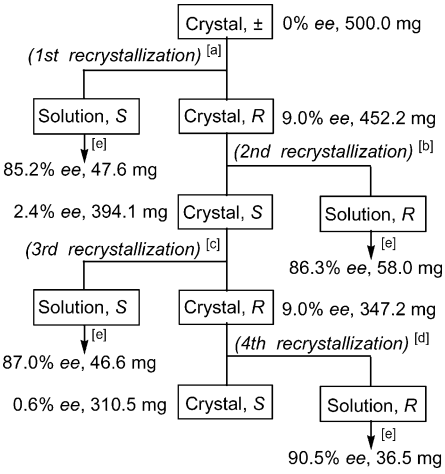

Figure 5. Preferential enrichment of (±)-**1b**. Conditions: [a] EtOH (1.3 mL), –20 °C, 7 d; [b] EtOH (1.2 mL), –20 °C, 7 d; [c] EtOH (1.0 mL), –20 °C, 7 d; [d] EtOH (0.9 mL), –20 °C, 7 d; [e] removal of the solvent by evaporation.

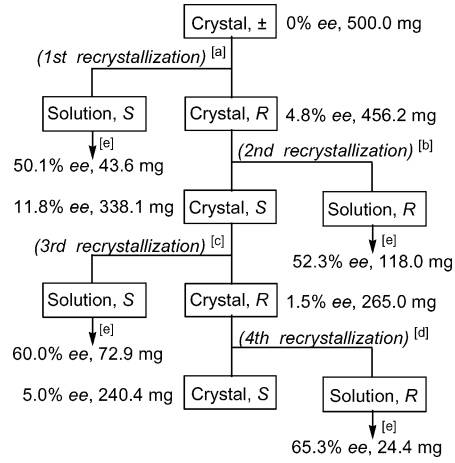

Figure 6. Preferential enrichment of (±)-**1c**. Conditions: [a] EtOH (0.7 mL), –20 °C, 30 d; [b] EtOH (0.7 mL), –20 °C, 21 d; [c] EtOH (0.5 mL), –20 °C, 21 d; [d] EtOH (0.4 mL), –20 °C, 21 d; [e] removal of the solvent by evaporation.

Crystal Structure

To clarify the relationship between the crystal structure and the occurrence of preferential enrichment, single crystals suitable for X-ray crystallographic analyses were prepared from the twofold supersaturated EtOH solutions at 20 °C for the stable forms of (±)-**1c**, (±)-**1d**, and (±)-**2a** (Table 2; Figures 7, 9, and 10).

The crystal structure of (±)-**1c** was a δ-form that has very often been observed for compounds showing preferential enrichment (Figure 7).[1–3] It is characterized by a centrosymmetric cyclic dimer of type A, which is formed by hydrogen bonding between the two hydroxy groups and the two terminal ethoxy groups in a pair of *R* and *S* enantiomers (O···O distance 2.921 Å). Another centrosymmetric cyclic dimer of type B is formed by (i) additional hydrogen bonds between the two sulfonate ions and the two nearest amide NHs (O···N distance 2.894 Å) and (ii) the electrostatic interactions between other oxygen atoms of the same sulfonate ions and the ammonium nitrogen atoms in the two neighboring long-chain cations ($O^{-}\cdots N^{+}$ distance 3.867 Å). Thus, the alternate alignment of the type A and type B cyclic dimers forms a heterochiral 1D chain. Furthermore, each 1D chain interacts with two adjacent 1D chains through other weak electrostatic interactions between the third oxygen atoms of the same sulfonate ions and the ammonium nitrogen atoms ($O^{-}\cdots N^{+}$ distance 4.370 Å) in the adjacent 1D chains to form a weak heterochiral 2D sheet structure. Similarly, the crystal structures of the stable forms of (±)-**1a** and (±)-**1b** were most likely to be a δ-form, because they showed an X-ray powder diffraction pattern (Figure 8) and an ATR-FTIR spectrum (Figure 11b) that were similar to those of (±)-**1c**.

The crystal structure of the β-form of (±)-**1d** is characterized by a heterochiral 1D chain consisting of two types of centrosymmetric cyclic dimers (type B and type C); type C is formed by the hydrogen bonds between (i) the two hydroxy groups and the two sulfonate ions (O···O distance

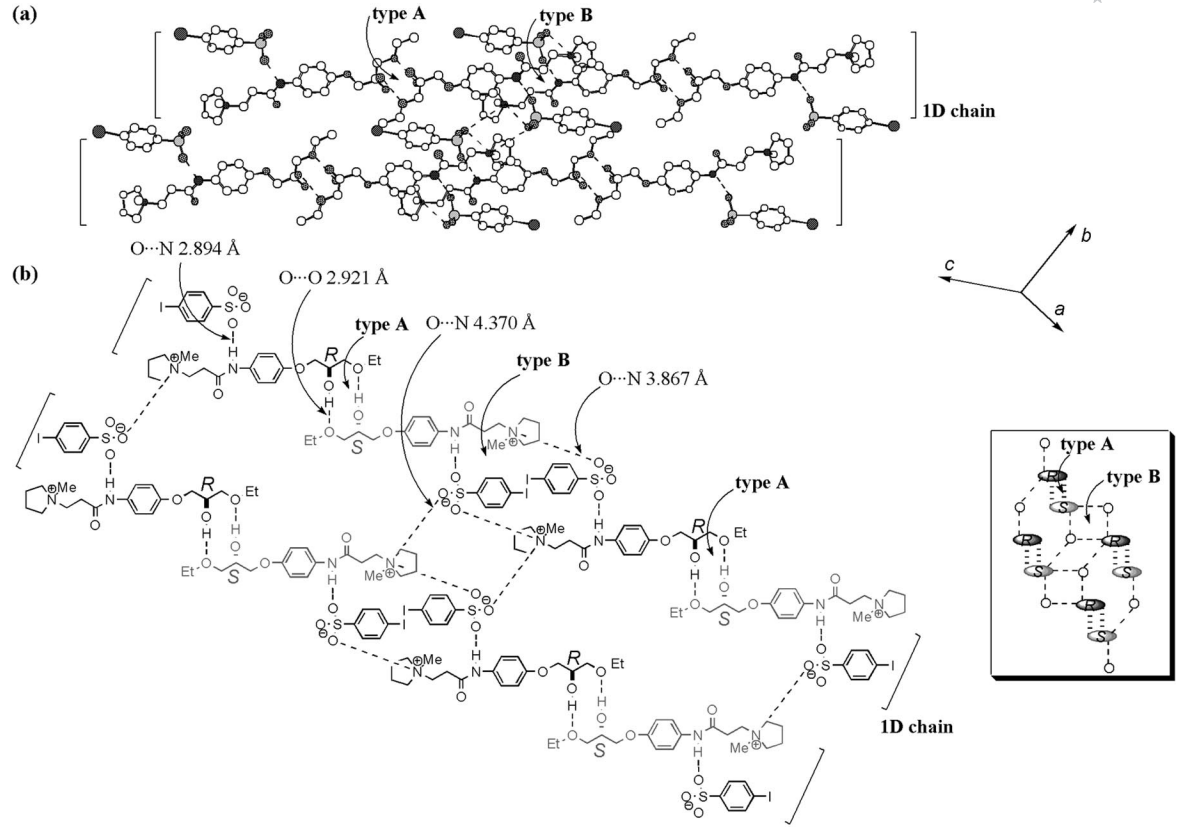

Figure 7. (a) Crystal structure of the δ-form of (±)-**1c**; carbon atoms are represented by white circles, whereas nonwhite circles represent oxygen, nitrogen, sulfur, and iodine atoms; (b) schematic representation of the intermolecular interactions in the same δ-form crystal.

2.849 Å) and (ii) other oxygen atoms of the same sulfonate ions and the two nearest amide NHs (O···N distance: 2.835 Å) in a pair of *R* and *S* enantiomers (Figure 9). The 1D chain interacts with two adjacent 1D chains through the C–H···O interaction between the methyl group of the *p*-toluenesulfonate ion and an amide C=O (C···O distance 3.474 Å). The crystal structure of the stable form of (±)-**2d** was judged to be a β-form, because of the similarity in the X-ray powder diffraction pattern (Figure S1) and the ATR-FTIR spectrum (Figure 11c) between (±)-**1d** and (±)-**2d**.

The crystal structure of the α_2-form of (±)-**2a** consists of two unique intermolecular interactions (Figure 10): one is a centrosymmetric cyclic dimer of type D and the other is a 2D sheet structure that is composed of only the symmetry-related sulfonate ions. The type D cyclic dimer is formed by hydrogen bonds between the two hydroxy groups and the two amide carbonyl groups in a pair of *R* and *S* enantiomers (O···O distance 2.927 Å). The sulfonate 2D sheet is formed by two types of hydrogen bonds between the two oxygen atoms of one sulfonate ion and the two *meta* hydrogen atoms in the neighboring sulfonate ions (O···C distances 3.051 Å and 3.259 Å; Figure 10c). Furthermore, the type D cyclic dimer is sandwiched by the two adjacent sulfonate 2D sheets through (i) the electrostatic interactions between the sulfonate oxygen atoms and the ammonium nitrogen atoms ($O^{-}\cdots N^{+}$ distance 4.404 Å) and (ii) the hydrogen bonds between other oxygen atoms of the same sulfonate ions and the amide NHs (O···N distance 2.813 Å; Figure 10b). The crystal structures of the stable form of (±)-**2b** and (±)-**2c** were assumed to take an α_2-polymorph by judging from comparison of X-ray powder diffraction patterns (Figure S2) and the ATR-FTIR spectra (Figure 11d) of (±)-**2a**–**c**.

Mechanism of Polymorphic Transition

To learn the mode of polymorphic transition, we monitored the crystallization process by in situ ATR-FTIR spectroscopy.[3,8,9,10] The individual spectra measured in the supersaturated EtOH solutions were compared with those in suspension after completion of crystallization and those in the solid state (Figures 11, S3, and S4). Consequently, the spectra measured before and after crystallization were quite different from each other. The spectra in the supersaturated solution indicated that all eight racemates took a similar γ-form supramolecular structure, which exhibited a characteristic S–O stretching vibration at around $\tilde{\nu}$ = 1190, 1220, and 1240 cm^{-1} (Figures 11a, S3, and S4), as reported previously.[3,8,9] The γ-form molecular assembly of (±)-**1a** in solution was gradually transformed into the metastable γ-form crystal and then the stable δ-form during crystallization (Figure 11a).

We already showed that the most important process in the mechanism of preferential enrichment was the polymor-

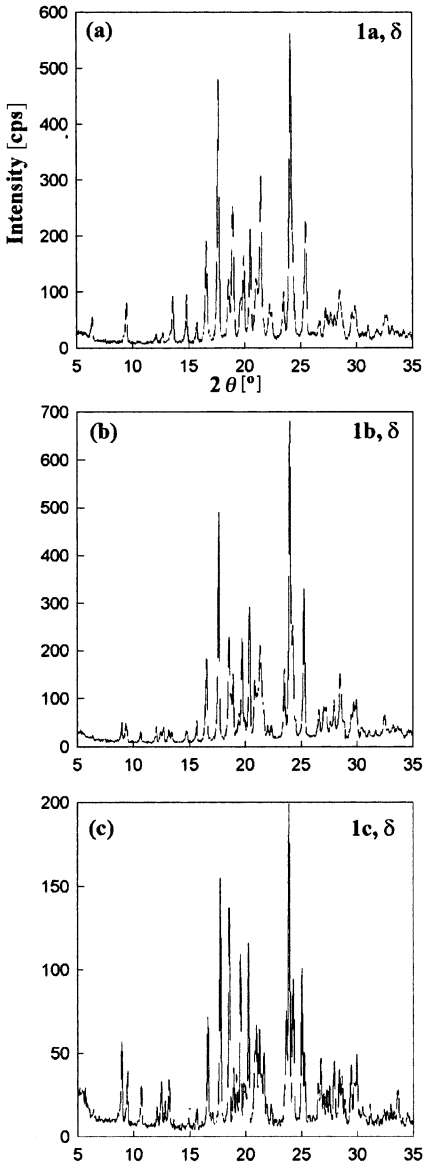

Figure 8. Powder XRD patterns of (a) (±)-**1a**, (b) (±)-**1b**, and (c) (±)-**1c**.

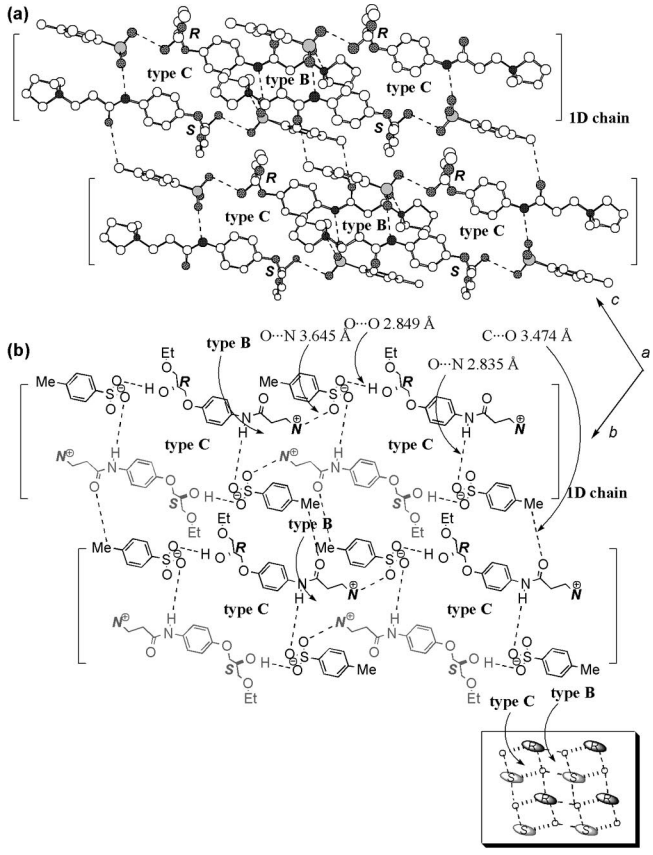

Figure 9. (a) Crystal structure of the β-form of (±)-**1d**; carbon atoms are represented by white circles, whereas nonwhite circles represent oxygen, nitrogen, and sulfur atoms; (b) schematic representation of the intermolecular interactions in the same β-form crystal; methyl groups in the ammonium groups were omitted for clarify.

phic transition of a metastable γ-form into the other stable polymorphs such as the δ-, ε-, and α_1-forms, followed by partial crystal disintegration inside the resulting crystals, which releases the slightly excess enantiomer in the initial crystals into solution.[1–3,6,8] Because the resulting partial crystal disintegration originates from the initial random arrangement of homochiral 1D chains in the metastable γ-form crystal, the crystals deposited immediately after the polymorphic transition should have a disordered molecular arrangement.[1–3] This is assured by the existence of disordered oxygen atoms [occupancy factors: 0.84 and 0.16 for O2(*S*) and O8(*r*), respectively] in the δ-form of (±)-**1c** (Figure 12). The distance between O1 and O8′(*s*) or O1′ and O8(*r*) in the disordered heterochiral type A dimer is 0.4 Å longer than that between O1 and O2′(*R*) or O1′ and O2(*S*). Thus, the partial crystal disintegration most likely occurs at the weakened heterochiral (*r,s*) dimer site in an area where an even number of homochiral *S* (*R*) chains were surrounded by two *R* (*S*) chains in the initial γ-form crystal, as reported previously (Figure 13).[1–3]

Although another type of heterochiral cyclic dimer (type C) was also seen in the β-form of (±)-**1d** (Figure 9), preferential enrichment did not occur. From the crystallographic analysis, the β-form of (±)-**1d** does not contain the disordered hydroxy groups that were observed in the δ-form of (±)-**1c**. Furthermore, the O···O distance (>8 Å) between the sulfonate oxygen atom and the hydroxy group (arrow *c*) in the initially formed γ-form crystal was known to be too long to induce solid-to-solid polymorphic transition for forming the cyclic dimer of type C (Figure 14).[3,8] From these facts, the γ-to-β polymorphic transition is most likely to occur in a solvent-mediated manner that cannot induce preferential enrichment.

In contrast, for (±)-**2a**–**c**, the polymorphic transition of the γ-form into the α_2-form was accompanied by a change in the space group from $P\bar{1}$ to $P2_1/n$. Therefore, half molecules of each enantiomer in the γ-form crystal need to turn to the opposite direction in order to generate the screw symmetry. Because such a drastic molecular motion cannot occur in the solid state, a solvent-mediated polymorphic tran-

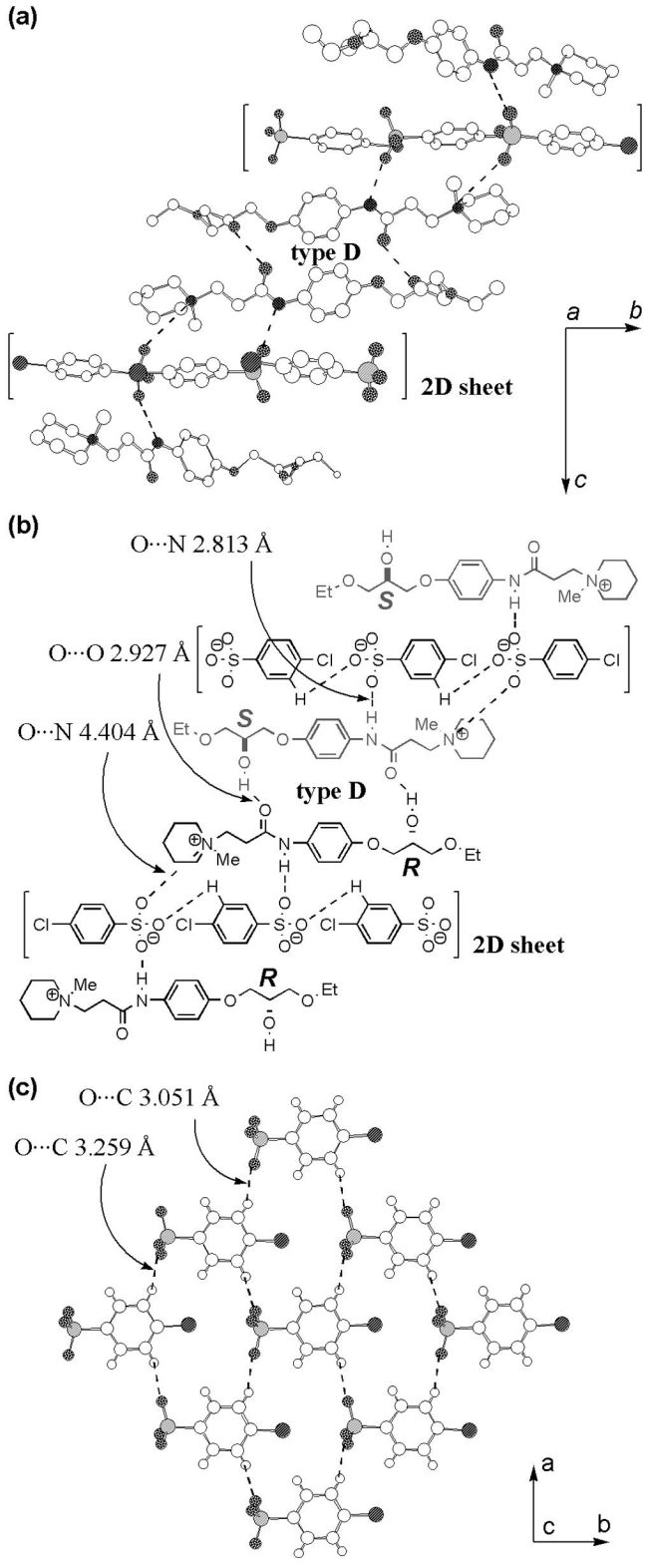

Figure 10. (a) Crystal structure of the α_2-form of (±)-**2a**; carbon atoms are represented by white circles, whereas nonwhite circles represent oxygen, nitrogen, sulfur, and chlorine atoms; (b) schematic representation of the intermolecular interactions in the same α_2-form crystal; (c) 2D sheet structure formed by the sulfonate ions in the *ab* plane.

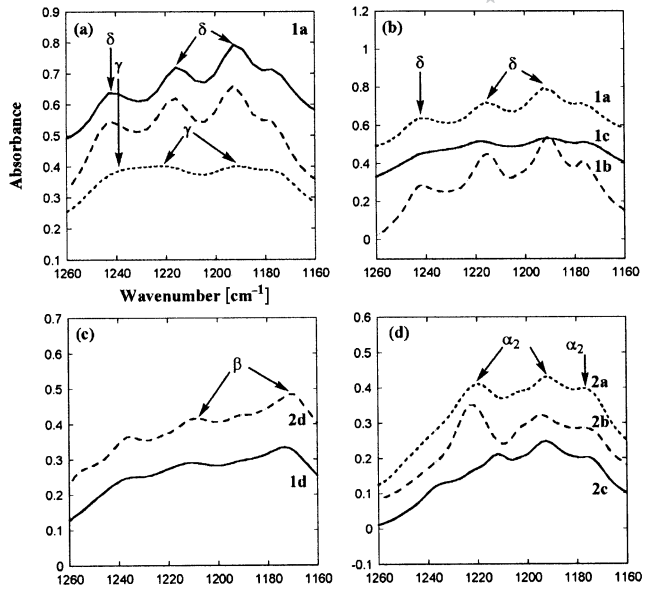

Figure 11. ATR-FTIR spectra (a) during crystallization from the supersaturated EtOH solution of (±)-**1a** at the beginning (dotted line,····) and the end (broken line, – –) of crystallization, with the spectrum in the solid state of the δ-form (solid line, ——); (b) in the solid state of the δ-form of (±)-**1a**–**c**; (c) in the solid state of the β-form of (±)-**1d** and (±)-**2d**; (d) in the solid state of the α_2-form of (±)-**2a**–**c**.

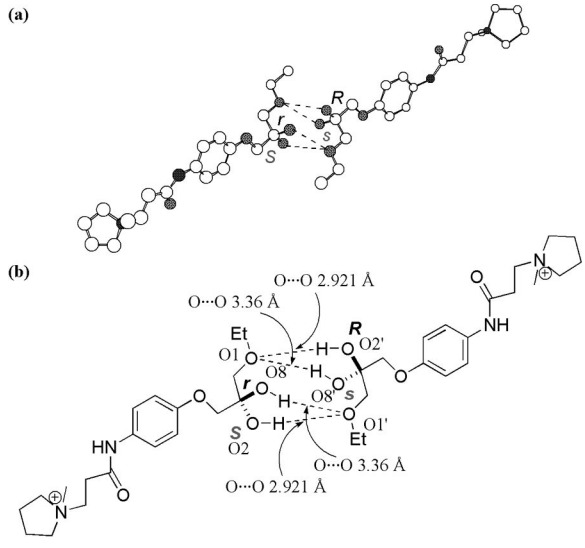

Figure 12. (a) Type A cyclic dimer structure of (±)-**1c** with orientational disorder at the position of the hydroxy group on an asymmetric carbon atom and (b) its schematic representation.

sition, which cannot induce preferential enrichment, should occur. The reason why the *N*-methylpiperidinium analogues showed such an undesired polymorphic transition can be explained in terms of the steric hindrance of a larger piperidinium ring than a pyrrolidinium ring to prevent the γ-to-δ transition ***a*** (Figure 14).

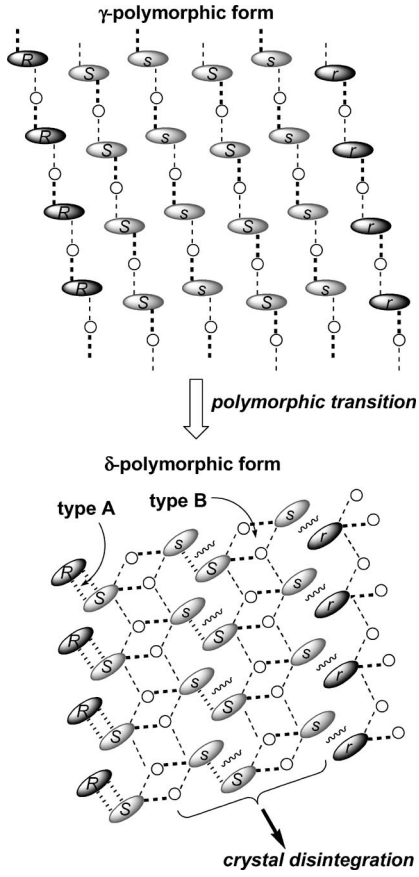

Figure 13. Polymorphic transition of the metastable γ-form into the stable δ-form, which is essential for the occurrence of preferential enrichment. This is a case in which an even number (four in this case) of homochiral *S* chains are surrounded by two *R* chains in the γ-form crystal, which results in partial crystal disintegration after polymorphic transition.

Conclusions

The effect of the structure of the cyclic ammonium group and the basicity of *p*-substituted benzenesulfonate ion on the mode of the polymorphic transition was investigated. Consequently, in order to induce the transition from the metastable γ-form into the δ-form through solvent-assisted solid-to-solid polymorphic transition, which is necessary to induce preferential enrichment, the steric size of the cyclic ammonium group must be small; otherwise, the solvent-mediated polymorphic transition occurs, which cannot induce preferential enrichment. Furthermore, the basicity of the sulfonate ion was found to be crucial for the occurrence of preferential enrichment: (±)-**1d** and (±)-**2d**, having the more basic *p*-toluenesulfonate ion rather than the *p*-halobenzenesulfonate ion, showed the solvent-mediated polymorphic transition of the γ-form into the β-form, so that preferential enrichment did not occur. This can be explained in terms of the high basicity of the *p*-toluenesulfonate ion. However, thus far we have found three different modes of polymorphic transition that allow the occurrence of preferential enrichment, and it may be possible to find another mode of polymorphic transition inducing preferential enrichment for the compounds that failed to show preferential enrichment in this paper.

Experimental Section

Generals: Differential scanning calorimetry (DSC) was performed at a scanning rate of 5 °C min^{-1}. The in situ FTIR spectra in solution or suspension and the solid-state FTIR spectra were recorded by using the attenuated total reflection (ATR) method on ReactIR 4000. ^{1}H NMR spectra were recorded at 500 MHz, and ^{13}C NMR spectra were recorded at 126 MHz at 25 °C. HPLC analyses were performed by using a chiral stationary phase column (Daicel Chiralcel OD-H, 0.46 × 25 cm), a mixture of hexane, ethanol, trifluoroacetic acid, and diethylamine (800:200:5:1) as the mobile phase at a flow rate of 0.3 mL min^{-1} at 30.0 °C, and a UV/Vis spectrometer (254 nm) as the detector. Powder X-ray diffraction patterns were recorded at a continuous scanning rate of 1° 2θ min^{-1} by using Cu-K_α radiation (40 kV, 40 mA) with the intensity of diffracted X-rays being collected at intervals of 0.01° 2θ. A Ni filter was used for the removal of Cu-K_β radiation.

Preparation of Racemic 1a–d and 2a–d: (±)-1-Bromo-2-[4-(2-hydroxy-3-ethoxypropoxy)phenylcarbamoyl]ethane (**3**) was prepared according to the published procedure (Scheme 1).[11]

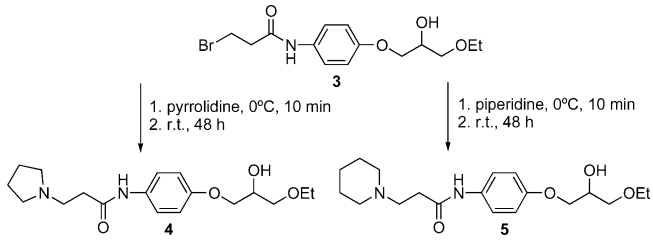

Scheme 1. Synthesis of amines **4** and **5**.

(±)-*N*-{2-[4-(2-Hydroxy-3-ethoxypropoxy)phenylcarbamoyl]ethyl}-pyrrolidine (4): To a mixture of **3** (8.00 g, 23 mmol) and water (80 mL) was added pyrrolidine (5 mL) dropwise over 10 min at 0 °C with stirring. The reaction mixture was warmed to room temperature and stirred vigorously for 48 h. The resulting mixture was extracted with CH_2Cl_2 (3 × 30 mL), and the combined organic phase was dried with anhydrous $MgSO_4$, filtered, and evaporated, followed by recrystallization from EtOH to give pure **4** as a colorless solid (6.83 g, 20 mmol, 87% yield). M.p. 132.1 °C (DSC). IR (KBr): $\tilde{\nu}$ = 3467, 2882, 2649, 1676, 1606, 1513, 1246, 1120, 1057 cm^{-1}. ^{1}H NMR (500 MHz,$CDCl_3$): δ = 1.22 (t, J = 7.0 Hz, 3 H), 1.85–1.89 (m, 4 H), 2.51 (dd, J = 5.1, 6.4 Hz, 2 H), 2.64–2.67 (m, 5 H), 2.83 (dd, J = 5.1, 6.4 Hz, 2 H), 3.53–3.59 (m, 3 H), 3.62 (dd, J = 4.5, 9.8 Hz, 1 H), 3.97–4.03 (m, 2 H), 4.15 (m, 1 H), 6.86 (ddd, J = 1.8, 3.8, 10.2 Hz, 2 H), 7.40 (ddd, J = 1.8, 3.8, 10.2 Hz, 2 H), 11.04 (s, 1 H) ppm. ^{13}C NMR (126 MHz, $CDCl_3$): δ = 15.1, 23.7, 24.6, 51.4, 53.1, 66.9, 69.1, 69.4, 71.3, 114.9, 121.1, 132.5, 154.8, 170.6 ppm. $C_{18}H_{28}N_2O_4 \cdot 0.4H_2O$ (343.63): C 62.91, H 8.45, N 8.15; found C 63.11, H 8.71, N 8.02.

(±)-*N*-{2-[4-(2-Hydroxy-3-ethoxypropoxy)phenylcarbamoyl]ethyl}-*N*-methylpyrrolidinium *p*-Chlorobenzenesulfonate [(±)-1a]: A mixture of **4** (2.00 g, 5.9 mmol) and methyl *p*-chlorobenzenesulfonate

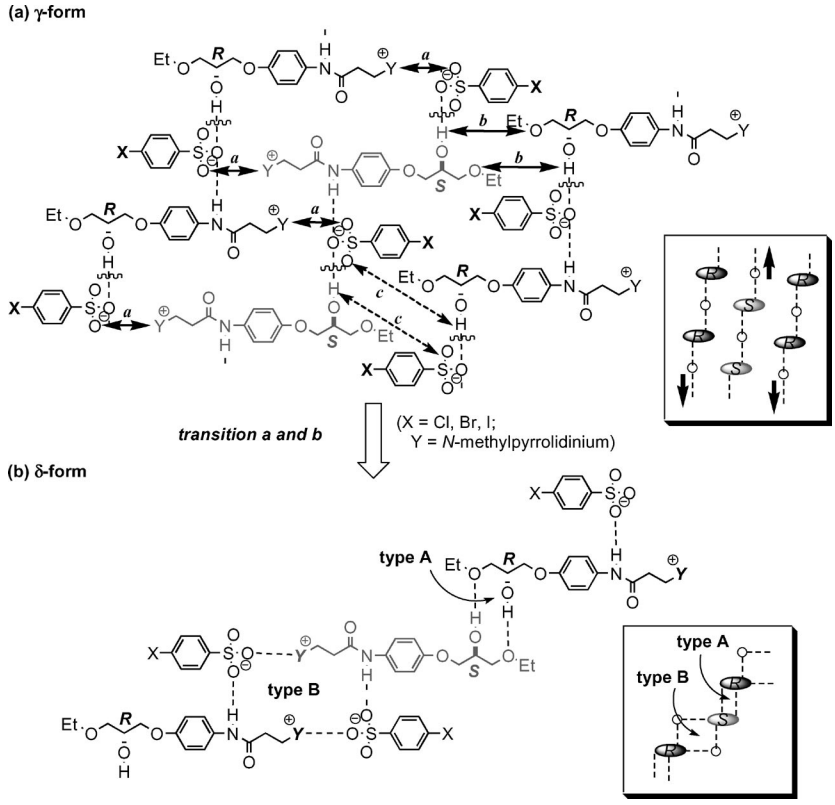

Figure 14. The mode of solvent-assisted solid-to-solid polymorphic transition of (a) a γ-form polymorph into (b) a δ-form polymorph. The arrows ***a*** and ***b*** indicate the sites of the formation of new electrostatic interactions or new hydrogen bonds, and the broken arrow ***c*** indicates the site of virtual rearrangement of hydrogen bonds necessary to form the β-form polymorph by a solvent-assisted solid-to-solid transition.

(1.35 g, 6.5 mmol) in acetone (20 mL) was heated under reflux for 24 h. The mixture was evaporated, and the resulting solid was washed with Et_2O. After drying in vacuo, (±)-**1a** (2.90 g, 5.3 mmol, 90% yield) was obtained as a colorless powder. M.p. 90.1 °C (DSC). IR (KBr): $\tilde{\nu}$ = 3424, 3083, 2871, 1679, 1557, 1514, 1219, 1100, 844 cm^{-1}. ^1H NMR (500 MHz, CD_3OD): δ = 1.18 (t, J = 7.0 Hz, 3 H), 2.23 (m, 4 H), 2.95 (t, J = 7.3 Hz, 2 H), 3.09 (s, 3 H), 3.52–3.59 (m, 8 H), 3.75 (t, J = 7.3 Hz, 2 H), 3.94 (dd, J = 5.6, 9.4 Hz, 1 H), 4.00–4.05 (m, 2 H), 6.90 (d, J = 9.0 Hz, 2 H), 7.41 (d, J = 9.0 Hz, 2 H), 7.44 (d, J = 9.0 Hz, 2 H), 7.78 (d, J = 9.0 Hz, 2 H) ppm. ^{13}C NMR (126 MHz, CD_3OD): δ = 15.4, 22.7, 31.8, 49.2 (overlapped with the solvent peak), 61.3 [t, J = 3.1 Hz (^{13}C-^{14}N coupling)], 65.8 [t, J = 3.1 Hz (^{13}C-^{14}N coupling)], 67.9, 70.3, 71.0, 72.8, 115.9, 123.0, 128.7, 129.5, 132.7, 137.1, 145.4, 157.4, 168.6 ppm. $C_{25}H_{35}ClN_2O_7S$ (543.07): calcd. C 55.29, H 6.50, N 5.16; found C 55.36, H 6.40, N 5.15.

(±)-**1b**, (±)-**1c**, and (±)-**1d** were prepared in an analogous way to the synthesis of (±)-**1a**.

(±)-*N*-{2-[4-(2-Hydroxy-3-ethoxypropoxy)phenylcarbamoyl]ethyl}-*N*-methylpyrrolidinium *p*-Bromobenzenesulfonate [(±)-1b]: M.p. 100.4 °C (DSC). IR (KBr): $\tilde{\nu}$ = 3438, 3080, 2869, 1679, 1558, 1513, 1245, 1117, 844 cm^{-1}. ^1H NMR (500 MHz, CD_3OD): δ = 1.18 (t, J = 7.0 Hz, 3 H), 2.23 (m, 4 H), 2.95 (t, J = 7.3 Hz, 2 H), 3.08 (s, 3 H), 3.52–3.59 (m, 8 H), 3.74 (t, J = 7.3 Hz, 2 H), 3.94 (dd, J = 5.6, 9.4 Hz, 1 H), 4.00–4.05 (m, 2 H), 6.90 (d, J = 9.1 Hz, 2 H), 7.44 (d, J = 9.1 Hz, 2 H), 7.57 (d, J = 8.7 Hz, 2 H), 7.71 (d, J = 8.7 Hz, 2 H) ppm. ^{13}C NMR (126 MHz, CD_3OD): δ = 15.4, 22.7, 31.8, 49.2 (overlapped with the solvent peak), 61.2 [t, J = 3.1 Hz (^{13}C-^{14}N coupling)], 65.8 [t, J = 3.1 Hz (^{13}C-^{14}N coupling)], 67.9, 70.3, 70.9, 72.7, 115.9, 123.0, 125.3, 128.9, 132.5, 132.7, 145.8, 157.4, 168.6 ppm. $C_{25}H_{35}BrN_2O_7S$ (587.52): calcd. C 51.11, H 6.00, N 4.77; found C 51.00, H 5.87, N 4.69.

(±)-*N*-{2-[4-(2-Hydroxy-3-ethoxypropoxy)phenylcarbamoyl]ethyl}-*N*-methylpyrrolidinium *p*-Iodobenzenesulfonate [(±)-1c]: M.p. 102.2 °C (DSC). IR (KBr): $\tilde{\nu}$ = 3431, 3087, 2869, 1678, 1611, 1513, 1246, 1111, 843 cm^{-1}. ^1H NMR (500 MHz, CD_3OD): δ = 1.18 (t, J = 7.0 Hz, 3 H), 2.23 (br., 4 H), 2.95 (t, J = 7.3 Hz, 2 H), 3.09 (s, 3 H), 3.52–3.59 (m, 8 H), 3.75 (t, J = 7.3 Hz, 2 H), 3.94 (dd, J = 5.6, 9.4 Hz, 1 H), 4.00–4.06 (m, 2 H), 6.91 (d, J = 9.1 Hz, 2 H), 7.44 (d, J = 9.1 Hz, 2 H), 7.57 (d, J = 8.7 Hz, 2 H), 7.71 (d, J = 8.7 Hz, 2 H) ppm. ^{13}C NMR (126 MHz, CD_3OD): δ = 15.4, 22.7, 31.8, 49.2 (overlapped with the solvent peak), 61.2 [t, J = 3.1 Hz (^{13}C-^{14}N coupling)], 65.8 [t, J = 3.1 Hz (^{13}C-^{14}N coupling)], 67.9, 70.3, 71.0, 72.8, 97.1, 115.9, 123.0, 128.8, 132.7, 138.6, 146.4, 157.4, 168.6 ppm. $C_{25}H_{35}IN_2O_7S$ (634.52): calcd. C 47.32, H 5.56, N 4.41; found C 47.38, H 5.46, N 4.39.

(±)-*N*-{2-[4-(2-Hydroxy-3-ethoxypropoxy)phenylcarbamoyl]ethyl}-*N*-methylpyrrolidinium *p*-Toluenesulfonate [(±)-1d]: M.p. 105.7 °C (DSC). IR (KBr): $\tilde{\nu}$ = 3373, 3064, 2884, 1680, 1610, 1507, 1219, 1120, 837 cm^{-1}. ^1H NMR (500 MHz, CD_3OD): δ = 1.19 (t, J = 7.0 Hz, 3 H), 2.22 (m, 4 H), 2.35 (s, 3 H), 2.94 (t, J = 7.3 Hz, 2 H), 3.07 (s, 3 H), 3.51–3.59 (m, 8 H), 3.73 (t, J = 7.3 Hz, 2 H), 3.94 (dd, J = 5.6, 9.4 Hz, 1 H), 4.00–4.05 (m, 2 H), 6.90 (d, J = 9.0 Hz, 2 H), 7.21 (d, J = 8.0 Hz, 2 H), 7.44 (d, J = 9.0 Hz, 2 H), 7.70 (d, J = 8.0 Hz, 2 H) ppm. ^{13}C NMR (126 MHz, CD_3OD): δ = 15.4, 21.3, 22.6, 31.8, 49.2 (overlapped with the solvent peak), 61.2 [t, J

= 3.1 Hz (^{13}C-^{14}N coupling)], 65.8 [t, J = 3.1 Hz (^{13}C-^{14}N coupling)], 67.9, 70.3, 70.9, 72.7, 115.8, 123.0, 127.0, 129.8, 132.8, 141.7, 143.7, 157.4, 168.6 ppm. $C_{26}H_{38}N_2O_7S$ (522.65): calcd. C 59.75, H 7.33, N 5.36; found C 59.57, H 7.37, N 5.18.

(±)-*N*-{2-[4-(2-Hydroxy-3-ethoxypropoxy)phenylcarbamoyl]ethyl}-piperidine (5): To a mixture of **3** (6.00 g, 17 mmol) and water (60 mL) was added piperidine (5 mL) dropwise over 10 min at 0 °C with stirring. The reaction mixture was warmed to room temperature and stirred vigorously for 48 h. The resulting mixture was extracted with CH_2Cl_2 (3 × 30 mL), and the combined organic phase was dried with anhydrous $MgSO_4$, filtered, and evaporated, followed by recrystallization from EtOH to give pure **5** as a colorless solid (4.86 g, 14 mmol, 82% yield). M.p. 94.2 °C (DSC). IR (KBr): $\tilde{\nu}$ = 3478, 2947, 2783, 1681, 1606, 1517, 1246, 1122, 1058 cm^{-1}. ^{1}H NMR (500 MHz, $CDCl_3$): δ = 1.22 (t, J = 7.0 Hz, 3 H), 1.54 (br., 2 H), 1.68 (quint, J = 5.5 Hz, 4 H), 2.49 (dd, J = 5.0, 6.9 Hz, 2 H), 2.53 (br., 4 H), 2.65 (dd, J = 5.0, 6.9 Hz, 2 H), 3.53–3.59 (m, 3 H), 3.62 (dd, J = 4.5, 9.8 Hz, 1 H), 3.97–4.03 (m, 2 H), 4.15 (quint, J = 5.4 Hz, 1 H), 6.88 (ddd, J = 1.8, 3.8, 10.2 Hz, 2 H), 7.46 (ddd, J = 1.8, 3.8, 10.2 Hz, 2 H), 11.20 (s, 1 H) ppm. ^{13}C NMR (126 MHz, $CDCl_3$): δ = 15.1, 24.3, 26.3, 32.5, 53.6, 54.4, 67.0, 69.2, 69.5, 71.3, 115.0, 120.9, 132.7, 154.8, 170.6 ppm. $C_{19}H_{30}N_2O_4 \cdot 0.3H_2O$ (355.86): C 64.13, H 8.67, N 7.87; found C 64.10, H 8.56, N 7.66.

(±)-**2a**, (±)-**2b**, (±)-**2c**, and (±)-**2d** were prepared in an analogous way to the synthesis of (±)-**1a**.

(±)-*N*-{2-[4-(2-Hydroxy-3-ethoxypropoxy)phenylcarbamoyl]ethyl}-*N*-methylpiperidinium *p*-Chlorobenzenesulfonate [(±)-2a]: M.p. 114.4 °C (DSC). IR (KBr): $\tilde{\nu}$ = 3428, 3081, 2870, 1672, 1613, 1513, 1225, 1119, 841 cm^{-1}. ^{1}H NMR (500 MHz, CD_3OD): δ = 1.19 (t, J = 7.0 Hz, 3 H), 1.68 (m, 2 H), 1.91 (quint, J = 5.7 Hz, 4 H), 2.91 (t, J = 7.3 Hz, 2 H), 3.08 (s, 3 H), 3.40 (t, J = 5.8 Hz, 4 H), 3.52–3.59 (m, 4 H), 3.74 (t, J = 7.3 Hz, 2 H), 3.93 (dd, J = 5.6, 9.4 Hz, 1 H), 4.00–4.06 (m, 2 H), 6.90 (d, J = 9.1 Hz, 2 H), 7.41 (d, J = 8.7 Hz, 2 H), 7.43 (d, J = 9.1 Hz, 2 H), 7.78 (d, J = 8.7 Hz, 2 H) ppm. ^{13}C NMR (126 MHz, CD_3OD): δ = 15.4, 21.0, 22.0, 30.1, 48.3, 61.0, 62.6, 67.9, 70.3, 71.0, 72.8, 115.9, 123.0, 128.7, 129.4, 132.7, 137.1, 145.4, 157.4, 168.6 ppm. $C_{26}H_{37}ClN_2O_7S$ (557.10): calcd. C 56.05, H 6.69, N 5.03; found C 56.16, H 6.53, N 5.04.

(±)-*N*-{2-[4-(2-Hydroxy-3-ethoxypropoxy)phenylcarbamoyl]ethyl}-*N*-methylpiperidinium *p*-Bromobenzenesulfonate [(±)-2b]: M.p. 116.5 °C (DSC). IR (KBr): $\tilde{\nu}$ = 3428, 3078, 2868, 1672, 1609, 1507, 1222, 1116, 839 cm^{-1}. ^{1}H NMR (500 MHz, CD_3OD): δ = 1.19 (t, J = 7.0 Hz, 3 H), 1.68 (m, 2 H), 1.92 (quint, J = 5.7 Hz, 4 H), 2.91 (t, J = 7.3 Hz, 2 H), 3.08 (s, 3 H), 3.40 (t, J = 5.8 Hz, 4 H), 3.52–3.59 (m, 4 H), 3.74 (t, J = 7.3 Hz, 2 H), 3.93 (dd, J = 5.6, 9.4 Hz, 1 H), 4.00–4.05 (m, 2 H), 6.90 (d, J = 9.1 Hz, 2 H), 7.44 (d, J = 9.1 Hz, 2 H), 7.57 (d, J = 8.7 Hz, 2 H), 7.72 (d, J = 8.7 Hz, 2 H) ppm. ^{13}C NMR (126 MHz, CD_3OD): δ = 15.4, 21.0, 22.0, 30.1, 48.3, 60.9, 62.6, 67.9, 70.2, 70.9, 72.7, 115.9, 123.0, 125.3, 128.9, 132.5, 132.7, 145.8, 157.4, 168.6 ppm. $C_{26}H_{37}BrN_2O_7S$ (601.55): calcd. C 51.91, H 6.20, N 4.66; found C 51.61, H 6.01, N 4.46.

(±)-*N*-{2-[4-(2-Hydroxy-3-ethoxypropoxy)phenylcarbamoyl]ethyl}-*N*-methylpiperidinium *p*-Iodobenzenesulfonate [(±)-2c]: M.p. 118.6 °C (DSC). IR (KBr): $\tilde{\nu}$ = 3421, 3080, 2866, 1671, 1610, 1507, 1211, 1112, 833 cm^{-1}. ^{1}H NMR (500 MHz, CD_3OD): δ = 1.19 (t, J = 7.0 Hz, 3 H), 1.68 (m, 2 H), 1.91 (quint, J = 5.7 Hz, 4 H), 2.91 (t, J = 7.3 Hz, 2 H), 3.08 (s, 3 H), 3.39 (t, J = 5.8 Hz, 4 H), 3.52–3.59 (m, 4 H), 3.74 (t, J = 7.3 Hz, 2 H), 3.94 (dd, J = 5.6, 9.4 Hz, 1 H), 4.00–4.06 (m, 2 H), 6.90 (d, J = 9.1 Hz, 2 H), 7.44 (d, J = 9.1 Hz, 2 H), 7.56 (d, J = 8.7 Hz, 2 H), 7.77 (d, J = 8.7 Hz, 2 H) ppm. ^{13}C NMR (126 MHz, CD_3OD): δ = 15.4, 21.0, 22.0, 30.1, 48.3, 60.9, 62.6, 67.9, 70.3, 70.9, 72.8, 97.1, 115.9, 123.0, 128.8, 132.7, 138.6, 146.4, 157.4, 168.6 ppm. $C_{26}H_{37}IN_2O_7S$ (648.55): calcd. C 48.15, H 5.75, N 4.32; found C 48.23, H 5.60, N 4.33.

(±)-*N*-{2-[4-(2-Hydroxy-3-ethoxypropoxy)phenylcarbamoyl]ethyl}-*N*-methylpiperidinium *p*-Toluenesulfonate [(±)-2d]: M.p. 120.6 °C (DSC). IR (KBr): $\tilde{\nu}$ = 3364, 3067, 2870, 1689, 1612, 1508, 1222, 1120, 841 cm^{-1}. ^{1}H NMR (500 MHz, CD_3OD): δ = 1.19 (t, J = 7.0 Hz, 3 H), 1.67 (m, 2 H), 1.90 (quint, J = 5.7 Hz, 4 H), 2.35 (s, 3 H), 2.91 (t, J = 7.3 Hz, 2 H), 3.07 (s, 3 H), 3.38 (t, J = 5.8 Hz, 4 H), 3.52–3.59 (m, 4 H), 3.72 (t, J = 7.3 Hz, 2 H), 3.94 (dd, J = 5.6, 9.4 Hz, 1 H), 4.00–4.06 (m, 2 H), 6.90 (d, J = 9.1 Hz, 2 H), 7.21 (d, J = 8.0 Hz, 2 H), 7.44 (d, J = 9.1 Hz, 2 H), 7.70 (d, J = 8.0 Hz, 2 H) ppm. ^{13}C NMR (126 MHz, CD_3OD): δ = 15.4, 21.0, 21.3, 22.0, 30.1, 48.3, 61.0, 62.6, 67.9, 70.3, 70.9, 72.7, 115.9, 123.0, 127.0, 129.8, 132.8, 141.7, 143.7, 157.4, 168.6 ppm. $C_{27}H_{40}N_2O_7S$ (536.68): calcd. C 60.42, H 7.51, N 5.22; found C 60.34, H 7.62, N 5.23.

General Procedure for the Preferential Enrichment Experiment of (±)-1a, (±)-1b, and (±)-1c (Figure 4)**: (±)-1a** (1.15 M, 500.0 mg, 0.921 mmol) was dissolved in EtOH (0.8 mL) on heating. The resulting threefold supersaturated solution was allowed to stand at –20 °C, and the *ee* value of the mother liquor was measured occasionally. The solution was left until the *ee* value reached equilibrium after the crystals were deposited. Consequently, it took 7 d for the first recrystallization. The deposited crystals were separated from the mother liquor by filtration. After evaporation of the solvent, *S*-enriched **1a** (50.2 mg, 75.0% *ee*) was obtained as a viscous colorless oil. The slightly *R*-enriched deposited crystals (449.6 mg, 8.4% *ee*) were subsequently recrystallized from EtOH (0.7 mL) in a similar manner, which led to the deposition of antipodal *S*-rich crystals (390.3 mg, 2.4% *ee*) and the enrichment of the *R* enantiomer in the mother liquor, from which *R*-enriched **1a** (59.2 mg, 79.5% *ee*) was obtained as a viscous oil. Similar crystallizations were repeated four times in all.

An analogous procedure was use for (±)-**1b** (Figure 5) and (±)-**1c** (Figure 6).

For reference, (*S*)-enriched **1a**–**c** were synthesized from commercially available (*S*)-epichlorohydrin. (*S*)-**1a** (90.9% *ee*): $[\alpha]_D^{20}$ = +1.84(1) (*c* = 2.138, MeOH); (*S*)-**1b** (90.9% *ee*): $[\alpha]_D^{20}$ = +1.41(2) (*c* = 2.137, MeOH); (*S*)-**1c** (93.6% *ee*): $[\alpha]_D^{20}$ = +1.97(2) (*c* = 2.136, MeOH).

X-ray Crystallographic Analysis of the δ-Form of 1c, the β-Form of 1d, and the α_2-Form of 2a: For the X-ray crystallographic analysis, the single crystal was mounted in a sealed capillary. The data collections were performed at 296 K with an Enraf–Nonius Kappa CCD diffractometer with graphite monochromated Mo-K_α radiation for the δ-form of (±)-**1c**, at 296 K with a Rigaku CCD diffractometer with graphite monochromated Mo-K_α radiation for the β-form of (±)-**1d**, and at 173 K with a Rigaku RAXIS RAPID diffractometer with graphite monochromated Mo-K_α radiation for the α_2-form of (±)-**2a**. All of the crystallographic calculations were performed by using the CrystalStructure software package of Rigaku and Rigaku/MSC. The crystal structures were solved by direct methods and refined by using full-matrix least-squares. All non-hydrogen atoms were refined anisotropically. The summary of the fundamental crystal data and experimental parameters for the structure determination is given in Table 2. CCDC-679608 [for (±)-**1c**], -679609 [for (±)-**1d**], and -679610 [for(±)-**2a**] contain the supplementary crystallographic data for this paper. These data can be obtained free of charge from The Cambridge Crystallographic Data Centre via www.ccdc.cam.ac.uk/data_request/cif.

Table 2. X-ray analytical data for (±)-**1c**, (±)-**1d**, and (±)-**2a**.

Compounds	**1c**	**1d**	**2a**
Polymorphic form	δ	*β*	α_2
Crystal system	triclinic	triclinic	monoclinic
Space group	$P\bar{1}$	$P\bar{1}$	$P2_1/n$
a [Å]	9.454(1)	9.1465(7)	10.3214(5)
b [Å]	10.4043(8)	13.705(2)	10.1843(6)
c [Å]	14.658(2)	12.1298(12)	25.5920(15)
α [°]	107.619(6)	111.098(4)	90
β [°]	96.572(6)	98.574(6)	95.0494(18)
γ [°]	92.618(7)	104.609(6)	90
V [Å^3]	1360.2(3)	1323.4(3)	2679.7(3)
Z	2	2	4
R[a], R_w[b]	0.0470, 0.0600	0.086, 0.142	0.0604, 0.0791

[a] $R = \Sigma||F_o| - |F_c||/\Sigma|F_o|$ for $I > 3.0\sigma(I)$ data. [b] $R_w = [\Sigma|c\,Y^{sim}(2\theta_i) - I^{exp}(2\theta_i) - Y^{back}(2\theta_i)|]/\Sigma|I^{exp}(2\theta_i)|$.

Supporting Information (see footnote on the first page of this article): Powder XRD patterns of the β-form crystal of (±)-**1d** and (±)-**2d**; powder XRD patterns of the α_2-form crystal of (±)-**2a**–**c**; ATR-FTIR spectra of (±)-**1b**–**d** and (±)-**2a**–**d**; powder XRD patterns of (±)-**1c**, (±)-**1d**, and (±)-**2a** obtained experimentally and simulated from the X-ray crystallographic data.

Acknowledgments

The present work was supported by the Grand-in-Aid for Scientific Research from the Japan Society for the Promotion of Science (No. 15350023).

[1] R. Tamura, T. Ushio, "Preferential Enrichment: A Dynamic Enantiomeric Resolution Phenomenon Caused by Polymorphic Transition During Crystallization" in *Enantiomer Separation: Fundamentals and Practical Methods* (Ed.: F. Toda), Kluwer Academic Publishers, Dordrecht, **2004**, pp. 135–163.
[2] R. Tamura, H. Takahashi, D. Fujimoto, T. Ushio, *Top. Curr. Chem.* **2007**, *269*, 53–82.
[3] R. Tamura, D. Fujimoto, Z. Lepp, K. Misaki, H. Miura, H. Takahashi, T. Ushio, T. Nakai, K. Hirotsu, *J. Am. Chem. Soc.* **2002**, *124*, 13139–13153.
[4] M. Horiguchi, S. Okuhara, E. Shimano, D. Fujimoto, H. Takahashi, H. Tsue, R. Tamura, *Cryst. Growth Des.* **2007**, *7*, 1643–1652.
[5] M. Horiguchi, S. Okuhara, E. Shimano, D. Fujimoto, H. Takahashi, H. Tsue, R. Tamura, *Cryst. Growth Des.* **2008**, *8*, 540–548.
[6] H. Miura, T. Ushio, K. Nagai, D. Fujimoto, Z. Lepp, H. Takahashi, R. Tamura, *Cryst. Growth Des.* **2003**, *3*, 959–965.
[7] D. Fujimoto, R. Tamura, Z. Lepp, H. Takahashi, T. Ushio, *Cryst. Growth Des.* **2003**, *3*, 973–979.
[8] D. Fujimoto, H. Takahashi, T. Ariga, R. Tamura, *Chirality* **2006**, *18*, 188–195.
[9] R. Tamura, M. Mizuta, S. Yabunaka, D. Fujimoto, T. Ariga, S. Okuhara, N. Ikuma, H. Takahashi, H. Tsue, *Chem. Eur. J.* **2006**, *12*, 3515–3527.
[10] For polymorphic transition during crystallization of carboxylic acids, see R. J. Davey, G. Dent, R. K. Mughal, S. Parveen, *Cryst. Growth Des.* **2006**, *6*, 1788–1796.
[11] H. Takahashi, R. Tamura, T. Ushio, Y. Nakajima, K. Hirotsu, *Chirality* **1998**, *10*, 705–710.

Received: February 29, 2008
Published Online: May 27, 2008

